

Parallel Supercomputing PC Cluster and Some Physical Results in Lattice QCD*

LUO Xiang-Qian¹, MEI Zhong-Hao¹, Eric B. GREGORY¹,
YANG Jie-Chao², WANG Yu-Li², and LIN Yin²

¹*Department of Physics, Zhongshan University, Guangzhou 510275, China*

²*Guangdong National Communication Network Science and Technology Stock Co., Ltd,
Guangzhou 510080, China*

October 25, 2018

Abstract

We describe the construction of a high performance parallel computer composed of PC components, present some physical results for light hadron and hybrid meson masses from lattice QCD. We also show that the smearing technique is very useful for improving the spectrum calculations.

Keywords: Computational Physics, Parallel Computing, Lattice QCD

*This work is supported by the National Science Fund for Distinguished Young Scholars (19825117), Key Project of National Science Foundation (10235040), Guangdong Provincial Natural Science Foundation, National and Guangdong Ministries of Education, Ministry of Science and Technology, Foundation of Zhongshan University Advanced Research Center, and Guoxun (Guangdong National Communication Network) Ltd.

1 Introduction

The interests of the computational physics and high energy physics group[1] at the Zhongshan University (ZSU) cover such topics as lattice gauge theory[2, 3, 4, 5, 6, 7, 8, 9], supersymmetry[10], quantum instantons[11] and quantum chaos[13, 12]. All of these topics can be investigated through Monte Carlo simulation, but can be quite costly in terms of computing power. In order to do large scale numerical investigations of these topics, we require a corresponding development of our local computing resources.

The last two decades have ushered in the computer revolution for the consumer. In this period computers have moved from the domain of large companies, universities, and governments, to private homes and small businesses. As computational power has become more accessible, our demands and expectations for this power have increased accordingly.

We demand an ever-increasing amount of computational ability for business, communication, entertainment, and scientific research. This rapid rise in both the demand for computational ability as well as the increase of that capability itself have forced a continual redefinition of the concept of a “super computer.” The computational speed and ability of household computers now surpasses that of computers which helped guide men to the moon. The demarcation between super computers and personal computers has been further blurred in recent years by the high speed and low price of modern CPUs and networking technology and the availability of low cost or free software. By combining these three elements - all readily available to the consumer - one can assemble a true super computer that is within the budget of small research labs and businesses. This type of cluster is generally termed a Beowulf class computer. The idea was originally developed as a project at the US National Aeronautics and Space Administration[14].

We document the construction of a cluster of PCs, configured to be capable of parallel processing, and show the performance in lattice QCD simulations. We also present some results for the hadron masses from lattice QCD.

2 Construction of a Parallel Cluster

2.1 Computational Hardware

We built a cluster of 10 PC type computers, all the components of which we purchased at normal consumer outlets for computer equipment. The major difference in our computers from one likely to be found in a home or business is that each is equipped with two CPUs. This allows us to roughly double our processing power without the extra overhead cost for extra cases, power supplies, network cards, etc. Specifically, we have installed two 500MHz Pentium III processors in each motherboard. For the purposes of this report we will describe each computer as one “node” in the cluster; i.e., a node has two processors. Each node has its own local EIDE hard disk, in our case each has 10GB. This amount of space is not necessary, as the operating system requires less than one gigabyte per node, however the price of IDE hard disks has dropped so rapidly that it seems a reasonable way to add supplementary storage space to the cluster. Furthermore, each node is equipped with memory (at least 128MB), a display card, a 100Mbit/s capable fast Ethernet card, a CDROM drive and a floppy drive. These last two items are not an absolute

necessity as installation can be done over the network, but they add a great deal of convenience and versatility for a very modest cost.

One node is special and equipped with extra or enhanced components. The first node acts as a file server and has a larger (20GB) hard disk. This disk is the location of all the home directories associated with user accounts. The first node also has a SCSI adapter, for connecting external backup devices such as a tape drive.

What each computer does not have is a monitor, keyboard, and mouse. Monitors can easily be one of the most expensive components of a home computer system. For a cluster such as this one, the individual nodes are not intended for use as separate workstations. Most users access the cluster through network connections. We use a single console (one small monitor, a keyboard and mouse) for administrative tasks. It is handy when installing the operating system on a new node. In this situation we move the console cables to the particular node requiring configuration. Once we have installed communications programs such as telnet and ssh, it is almost never necessary to move the monitor and cables to the subordinate nodes.

2.2 Communications Hardware

There are many options for networking a cluster of computers, including various types of switches and hubs, cables of different types and communication protocol. We chose to use fast Ethernet technology, as a compromise between budget and performance demands. We have already stated that we equipped each node with a 100Mbit/s capable fast Ethernet card. A standard Ethernet hub has the limitation on not being able to accommodate simultaneous communications between two separate pairs of computers, so we use a fast Ethernet switch. This is significantly more expensive than a hub, but necessary for parallel computation involving large amounts of inter-node communication. We found a good choice to be a Cisco Systems 2900 series switch. For ten nodes a bare minimum is a 12 port switch: one port for each node plus two spare ports for connecting either workstations or a connection to an external network. We have in fact opted for a 24 port switch to leave room for future expansion of the cluster as our budget permits.

100Mbit per second communication requires higher quality “Category-5” Ethernet cable, so we use this as the connection between the nodes and the switch. It should be noted that while a connection can be made from one of the switch ports to an external Internet router, this cable must be “crossover” cable with the input and output wire strands switched. The general layout of the cluster hardware is shown in Figure 1.

2.3 Software

For our cluster we use the Linux open source UNIX-like operating system. Specifically, we have installed a Redhat Linux distribution, due to the ease of installation. The most recent Linux kernel versions automatically support dual CPU computers. Linux is also able to support a Network File System (NFS), allowing all of the nodes in the cluster to share hard disks, and a Network Information System (NIS), which standardizes the usernames and passwords across the cluster.

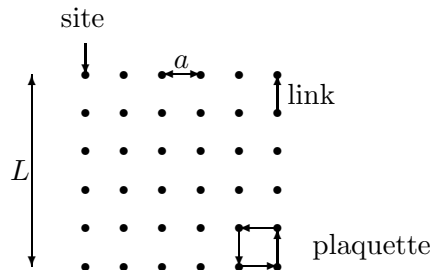
The one precaution one must take before constructing such a cluster is that the hardware components are compatible with Linux. The vast majority of PC type personal computers in the world are running a Windows operating system, and hardware manufacturers usually write

only Windows device drivers. Drivers for Linux are usually in the form of kernel modules and are written by Linux developers. As this is a distributed effort, shared by thousands of programmers worldwide, often working as volunteers, every PC hardware component available is not necessarily immediately compatible with Linux. Some distributions, such as Redhat have the ability to probe the hardware specifications during the installation procedure. It is rather important to check on-line lists of compatible hardware — particularly graphics cards and network cards — before purchasing hardware. We began by purchasing one node first and checking the compatibility with the operating system first before purchasing the rest of the nodes.

To provide parallel computing capability, we use an Message Passing Interface (MPI) implementation. MPI is a standard specification for message passing libraries[15]. Specifically we use the *mpich* implementation, which is available for free download over the world wide web[16]. An MPI implementation is a collection of software that allows communication between programs running on separate computers. It includes a library of supplemental *C* and *FORTRAN* functions to facilitate passing data between the different processors.

3 Basic Ideas of Lattice QCD

Our main purpose for building the PC cluster is to do large scale lattice Quantum Chromodynamics (QCD) simulations. The basic idea of lattice gauge theory[18], as proposed by K. Wilson in 1974, is to replace the continuous space and time by a discrete grid:



Gluons live on links $U(x, \mu) = e^{-ig \int_x^{x+\mu a} dx' A_\mu(x')}$, and quarks live on lattice sites. The continuum Yang-Mills action $S_g = \int d^4x \text{Tr} F_{\mu\nu}(x) F_{\mu\nu}(x)/2$ is replaced by

$$S_g = -\frac{\beta}{6} \sum_p \text{Tr}(U_p + U_p^\dagger - 2), \quad (1)$$

where $\beta = 6/g^2$, and U_p is the ordered product of link variables U around an elementary plaquette. The continuum quark action $S_q = \int d^4x \bar{\psi}^{cont}(x)(\gamma_\mu D_\mu + m)\psi^{cont}(x)$ is replaced by

$$S_q = \sum_{x,y} \bar{\psi}(x) M_{x,y} \psi(y). \quad (2)$$

For Wilson fermions, the quark field ψ on the lattice is related to the continuum one ψ^{cont} by $\psi = \psi^{cont} a^3 / (2\kappa)$ with $\kappa = 1/(2ma + 8)$. M is the fermionic matrix:

$$M_{x,y} = \delta_{x,y} - \kappa \sum_{\mu=1}^4 \left[(1 - \gamma_{\mu}) U_{\mu}(x) \delta_{x,y-\hat{\mu}} + (1 + \gamma_{\mu}) U_{\mu}^{\dagger}(x - \hat{\mu}) \delta_{x,y+\hat{\mu}} \right]. \quad (3)$$

For Kogut-Susskind fermions, the fermionic matrix is given by

$$\begin{aligned} M_{x,y} &= ma\delta_{x,y} + \frac{1}{2} \sum_{\mu=1}^4 \eta_{\mu}(x) \left[U_{\mu}(x) \delta_{x,y-\hat{\mu}} - U_{\mu}^{\dagger}(x - \hat{\mu}) \delta_{x,y+\hat{\mu}} \right], \\ \eta_{\mu}(x) &= (-1)^{x_1+x_2+\dots+x_{\mu-1}}. \end{aligned} \quad (4)$$

Physical quantities are calculable through Monte Carlo (MC) simulations with importance sampling. Fermion fields must be integrated out before the simulations, leading to

$$\langle F \rangle = \frac{\int [dU] \bar{F}([U]) e^{-S_g([U])} (\det M)^{N_f}}{\int [dU] e^{-S_g([U])} (\det M)^{N_f}} \approx \frac{1}{N_{\text{config}}} \sum_{\text{Conf}} \bar{F}[\text{Conf}]. \quad (5)$$

Here \bar{F} is the operator after Wick contraction of the fermion fields and the summation is over the gluonic configurations, Conf , drawn from the Boltzmann distribution. In quenched approximation, $\det(M) = 1$.

We introduce the u and d quark propagators

$$\begin{aligned} Q_{s_1 c_1, s_2 c_2}^u(x, y) &= M^{-1}[U, \kappa = \kappa_u]_{x s_1 c_1, y s_2 c_2}, \\ Q_{s_1 c_1, s_2 c_2}^d(x, y) &= M^{-1}[U, \kappa = \kappa_d]_{x s_1 c_1, y s_2 c_2}, \end{aligned} \quad (6)$$

where the Dirac and color indexes are explicitly written. In general, most of the computer time in the simulation of hadron masses or dynamical quarks is spent on the computations of the quark propagators. Usually these operations are accomplished by means of some inversion algorithm, which solves linear equation systems.

To compare with the real world, the continuum limit $a \rightarrow 0$ should be eventually taken. On the other hand, to keep the physical volume $(La)^3$ unchanged, the number of spatial lattice sites L^3 should be very large. To reliably measure the effective mass of a hadron, one has also to increase the number of temporal lattice sites T accordingly. Therefore, the computational task will then be tremendously increased. As such, it is well suited for parallelization. A parallel lattice QCD algorithm divides the lattice into sections and assigns the calculations relevant to each section to a different processor. Near the boundaries of the lattice sections, information must be exchanged between processors. However, since the calculations are generally quite local, the inter-processor communication is not extremely large.

4 Performance and Cost

We ran a standard LINPACK benchmark test and determined the peak speed of a single 500MHz Pentium III processor. The results of this test are shown in Table 1 to be about 100 million

Table 1: Results of LINPACK benchmark test on a single CPU.

| Precision | Mflop |
|-----------|----------|
| single | 86 - 114 |
| double | 62 - 68 |

| Interface directions | hypercubes (CPUs) | Lattice volume | Total interface | interface / CPU |
|----------------------|-------------------|-------------------------|-----------------|-----------------|
| j | 2^j | $L^{4-j} \times (2L)^j$ | $2^j j L^3$ | $j L^3$ |
| 0 | 1 | L^4 | 0 | 0 |
| 1 | 2 | $L^3 \times 2L$ | $2L^3$ | L^3 |
| 2 | 4 | $L^2 \times (2L)^2$ | $8L^3$ | $2L^3$ |
| 3 | 8 | $L \times (2L)^3$ | $24L^3$ | $3L^3$ |
| 4 | 16 | $(2L)^4$ | $64L^3$ | $4L^3$ |

Table 2: Summary of boundary sizes for division of a lattice into 1, 2, 4, 8 and 16 hypercubes of size L^4 .

floating point operations a second (Mflops). With this in mind, we can say that the theoretical upper limit for the aggregate speed of the whole cluster (20 CPUs) approaches 2 Gflops. Of course this is possible only in a computational task that is extremely parallelizable with minimum inter-node communications, no cache misses, etc. In the year 2000, the cost for our entire cluster was about US\$15,000, including the switch. This means that the cost for computational speed was about US\$7.50/Mflop. (Eliminating less essential hardware such as CDROMS, display cards, and floppy drives and using smaller hard disks on the subordinate nodes would further reduce this number.) It is instructive to compare this to other high performance computers. One example is a Cray T3E-1200. Starting at US\$630,000 for six 1200 Mflop processors[17], the cost is about US\$87.50 per Mflop. The Cray is more expensive by an order of magnitude. Clearly there are advantages in communication speed and other performance factors in the Cray that may make it more suitable for some types of problems. However, this simple calculation shows that PC clusters are an affordable way for smaller research groups or commercial interests to obtain a high performance computer.

A widely used lattice QCD simulation program is the MILC (MIMD Lattice Collaboration) code [19]. It has timing routines provided so that one can use the parallelized conjugate gradient (CG) routine for inverting the fermionic matrix in the simulation as a benchmark. Furthermore, as this code is very versatile and is designed to be run on a wide variety of computers and architectures. This enables quantitative comparison of our cluster to both other clusters and commercial supercomputers. In the MILC benchmark test we ran to a convergence tolerance of 10^{-5} per site. For consistency with benchmarks performed by others, we simulated Kogut-Susskind fermions given by Eq. (4).

We illustrate the result of the MILC code benchmark test in Figure 2. This figure deserves some explanation. We have run the benchmark test for different size lattices and different numbers

| L | single processor speed (Mflops) |
|-----|---------------------------------|
| 4 | 161.5 |
| 6 | 103.2 |
| 8 | 78.6 |
| 10 | 76.4 |
| 12 | 73.9 |
| 14 | 75.9 |

Table 3: Summary of single CPU performance.

of processors. It is useful to look at how performance is affected by the number of CPUs, when the amount of data per CPU is held fixed, that is each CPU is responsible for a section of the lattice that has L^4 sites. For one CPU, the size of the total lattice is L^4 . For two CPUs it is $L^3 \times 2L$. For four CPUs the total lattice is $L^2 \times (2L)^2$; for eight CPUs, $L \times (2L)^3$, and for 16 CPUs the total size of the lattice is $(2L)^4$.

Note that the falloff in performance with increased number of CPUs is dramatic. This is because inter-processor message passing is the slowest portion of this or any MPI program and from two to sixteen CPUs, the amount of communication per processor increases by a factor of four. Table 2 shows that for a lattice divided into 2^j hypercubes, each of size L^4 , there will be j directions in which the CPUs must pass data to their neighbors. The amount of communication each processor must perform is proportional to the amount of interface per processor. As this increases, per node performance decreases until $j = 4$ and every lattice dimension has been divided (for a $d = 4$ simulation), and the per-processor performance should remain constant as more processors are added. The shape of this decay is qualitatively consistent with $1/j$ falloff.

Of course there are other ways to divide a four-dimensional lattice. The goal of a particular simulation will dictate the geometry of the lattice and the therefore the most efficient way to divide it up (generally minimizing communication). A four-CPU simulation using a $4L \times L^3$ lattice has the four hypercubic lattice sections lined up in a row (as opposed to in a 2×2 square for a $L^2 \times (2L)^2$ lattice) and has the same amount of communication per CPU as does the $L^3 \times 2L$ two-CPU simulation. In a benchmark test the per-CPU performance was comparable to the performance in the two-CPU test.

For a single processor, there is a general decrease in performance as L increases, as shown in Tab. 3. This is well explained in [20] as due to the larger matrix size using more space outside of the cache memory, causing slower access time to the data.

For multiple CPUs there is in performance improvement as L is increased. The explanation for this is that the communication bandwidth is not constant with respect to message size, as Fig. 3 shows. For very small message sizes, the bandwidth is very poor. It is only with messages of around 10kB or greater that the bandwidth reaches the full potential of the fast Ethernet hardware, nearly 100Mbit/sec. With a larger L , the size of the messages is also, improving the communication efficiency. The inter-node communication latency for our system is $102\mu s$. As inter-node communication is the slowest part, a parallel program this far out-ways the effect of cache misses.

5 Physics Results

5.1 Green functions

Calculation of hadron spectroscopy remains to be an important task of non-perturbative studies of QCD using lattice methods. In this paper, we will present the spectrum results of light hadrons and 1^{-+} hybrid meson with quenched Wilson fermions. π , ρ , proton or Δ^{++} consists of quark and anti-quark, and their operators are given by:

$$\begin{aligned}
O^{\pi^+}(x) &= \bar{d}_{s_1 c}(x) \gamma_5 s_1 s_2 u_{s_2 c}(x), \\
O_k^{\rho^+}(x) &= \bar{d}_{s_1 c}(x) \gamma_k s_1 s_2 u_{s_2 c}(x), \\
O_{s_1}^p(x) &= \epsilon_{c_1 c_2 c_3} (C \gamma_5)_{s_2 s_3} u_{s_1 c_1}(x) (u_{s_2 c_2}(x) d_{s_3 c_3}(x) - d_{s_2 c_2}(x) u_{s_3 c_3}(x)), \\
O_{s_1}^{\Delta^{++}}(x) &= \epsilon_{c_1 c_2 c_3} (C \gamma_5)_{s_2 s_3} u_{s_1 c_1}(x) u_{s_2 c_2}(x) u_{s_3 c_3}(x),
\end{aligned} \tag{7}$$

where u and d are the ‘‘up’’ and ‘‘down’’ quark fields, C is the charge conjugation matrix, c is the color index of the Dirac field, and s is the Dirac spinor index. Summation over repeated index is implied. The correlation functions of a hadron is:

$$C_h(t) = \sum_{\vec{x}} \langle O_h^\dagger(\vec{x}, t) O_h(0, 0) \rangle, \tag{8}$$

where $O_h(\vec{x}, t)$ is a hadron operator given in (7). Then,

$$\begin{aligned}
C_{\pi^+}(t) &= -\langle \sum_{\vec{x}} \text{Tr}_{sc} (\gamma_5 Q_d(x, 0) \gamma_5 Q_u(0, x)) \rangle, \\
C_{\rho^+}(t) &= -\langle \sum_{\vec{x}} \text{Tr}_{sc} (\gamma_k Q_d(x, 0) \gamma_k Q_u(0, x)) \rangle, \\
C_p(t) &= \epsilon_{c_1 c_2 c_3} \epsilon_{c_4 c_5 c_6} (C \gamma_5)_{s_3 s_4} (C \gamma_5)_{s_5 s_6} \left(Q_{s_1 c_1, s_2 c_4}^u(x, y) Q_{s_3 c_2, s_5 c_5}^u(x, y) Q_{s_4 c_3, s_6 c_6}^d(x, y) \right. \\
&\quad \left. + Q_{s_1 c_1, s_5 c_4}^u(x, y) Q_{s_3 c_2, s_2 c_5}^u(x, y) Q_{s_4 c_3, s_6 c_6}^d(x, y) \right), \\
C_{\Delta^{++}}(t) &= \epsilon_{c_1 c_2 c_3} \epsilon_{c_4 c_5 c_6} (C \gamma_k)_{s_3 s_4} (C \gamma_k)_{s_5 s_6} \left(Q_{s_1 c_1, s_2 c_4}^u(x, y) Q_{s_3 c_2, s_5 c_5}^u(x, y) Q_{s_4 c_3, s_6 c_6}^u(x, y) \right. \\
&\quad \left. + 2 Q_{s_1 c_1, s_5 c_4}^u(x, y) Q_{s_3 c_2, s_2 c_5}^u(x, y) Q_{s_4 c_3, s_6 c_6}^u(x, y) \right),
\end{aligned} \tag{9}$$

where Tr_{sc} stands for a trace over spin and color. In Tab. 4, we list the operator for the P-wave a_1 meson, which is also made of quark and anti-quark.

Hybrid (exotic) mesons, which are important predictions of quantum chromodynamics (QCD), are states of quarks and anti-quarks bound by excited gluons. First principle lattice study of such states would help us understand the role of ‘‘dynamical’’ color in low energy QCD and provide valuable information for experimental search for these new particles. In Tab. 4, the operator of 1^{-+} meson is given.

For sufficiently large values of t and the lattice time period T , the correlation function is expected to approach the asymptotic form:

$$C_h(t) \rightarrow Z_h [\exp(-m_h a t) + \exp(m_h a t - m_h a T)]. \tag{10}$$

| meson | J^{PC} | Mnemonic | Operator |
|------------------------------------|----------------------|---------------------------------------|---|
| $\bar{q}q$ $f_1(\text{P-wave})$ | 1^{++} | ${}^3P_1 f_1$ | $\epsilon_{ijk} \bar{\psi} \gamma_j \overleftrightarrow{\partial}_k \psi$ |
| $\bar{q}qg$ 1^{-+} q^4 | 1^{-+} 1^{-+} | $\rho \otimes B$ $\pi \otimes a_1$ | $\bar{\psi}^{c_1} \gamma_j \psi^{c_2} F_{ji}^{c_1 c_2}$ $\bar{\psi}_{f_1}^{c_1}(\vec{x}) \gamma_5 \psi_{f_2}^{c_1}(\vec{x}) \bar{\psi}_{f_2}^{c_2}(\vec{y}) \gamma_5 \gamma_i \psi_{f_3}^{c_2}(\vec{y})$ |

Table 4: Source and sink operators for a_1 and hybrid mesons.

| volume | β | warmup | stored configs. |
|------------------|---------|--------|-----------------|
| $8^3 \times 32$ | 5.7 | 200 | 200 |
| $8^3 \times 32$ | 5.85 | 200 | 200 |
| $12^3 \times 36$ | 6.25 | 200 | 200 |
| $16^3 \times 32$ | 6.25 | 600 | 600 |

Table 5: Simulation parameters

Fitting the equation at large t , the effective mass of a hadron am_h is obtained.

5.2 Light hadron masses

We updated the pure SU(3) gauge fields with Cabibbo-Marinari quasi-heat bath algorithm, each iteration followed by 4 over-relaxation sweeps. The simulation parameters are listed in Tab. 5. The distance between two nearest stored configurations is 100. The auto-correlation time was computed to make sure that these configurations are independent.

The u quark and d quark are assumed to be degenerate. Using the CG algorithm, the quark propagators in Eq. (6) are calculated by inverting the Dirac matrix with preconditioning via ILU decomposition by checkerboards. The convergence tolerance we set is 5×10^{-8} . To extract masses from the hadron propagators, we must average the correlation function in Eq. (9) of the hadron over the ensemble of gauge configurations, and use a fitting routine to evaluate am_h in Eq. (10).

The quenched simulations were performed at lattice coupling of $\beta = 5.7$, $\beta = 5.85$ on the $8^3 \times 32$ lattice. We compared the results with those by MILC and GF11. At $\beta = 6.25$, we computed the light meson and baryon masses on the $12^3 \times 36$ and $16^3 \times 32$ lattices. The data for $\beta = 6.25$ have been reported in Ref. [23]. Here we detail the results for $\beta = 5.7$ and $\beta = 5.85$.

In Fig. 4, we show the pion correlation function at $\beta = 5.85$, and $\kappa = 0.1585$. In selecting the time range to be used in the fitting, we have tried to be systematic. We choose the best fitting range by maximizing the confidence level of the fit and optimizing $\chi^2/d.o.f$.

Point source means a delta function, and smeared source means a spread-out distribution (an approximation to the actual wave-function of the quantum state). For example, the simplest operator for a meson is just $O_h(\vec{x}) = \bar{q}(\vec{x})q(\vec{x})$, i.e. the product of quark and anti-quark fields at a single point. A disadvantage of this point source, is that this operator creates not only the lightest meson, but all possible excited states too. To write down an operator which creates more

| Particle | Group | Configs | Lattice | t_{min} | t_{max} | Mass | χ^2/dof | $C.L.$ |
|----------|-------|---------|------------------|-----------|-----------|-----------|--------------|--------|
| π | MILC | 90 | $16^3 \times 32$ | 7 | 16 | 0.378(2) | 12.38/8 | 0.135 |
| | ZSU | 200 | $8^3 \times 32$ | 8 | 16 | 0.379(6) | 8.74/7 | 0.163 |
| ρ | MILC | 90 | $16^3 \times 32$ | 8 | 16 | 0.530(3) | 2.857/7 | 0.898 |
| | ZSU | 200 | $8^3 \times 32$ | 8 | 16 | 0.533(7) | 4.67/7 | 0.216 |
| proton | MILC | 90 | $16^3 \times 32$ | 7 | 16 | 0.783(10) | 8.339/8 | 0.401 |
| | ZSU | 200 | $8^3 \times 32$ | 8 | 16 | 0.796(19) | 11.36/7 | 0.112 |
| Δ | MILC | 90 | $16^3 \times 32$ | 8 | 16 | 0.852(11) | 9.302/7 | 0.232 |
| | ZSU | 200 | $8^3 \times 32$ | 8 | 16 | 0.857(13) | 16.51/7 | 0.023 |

Table 6: Effective masses of light hadrons at $\beta=5.85$ and $\kappa=0.1585$ on the lattice $16^3 \times 32$ (MILC) and $8^3 \times 32$ (ZSU, this work).

of the single state, one must “smear” the operator out, e.g.

$$O_h(\vec{x}) = \sum_{\vec{y}} \bar{q}(\vec{x}) f(\vec{x} - \vec{y}) q(\vec{y}), \quad (11)$$

where $f(\vec{x})$ is some smooth function. Here we choose

$$f(\vec{x}) = N \exp(-|\vec{x}|^2/r_0^2), \quad (12)$$

with N a normalization factor. The size of the smeared operator should generally be comparable to the size of the hadron created. There is no automatic procedure for tuning the smearing parameter r_0 . One simply has to experiment with a couple of choices. We plot respectively in Figs. 5, 6, 7 and 8, the effective mass of π , ρ , proton and Δ particles, as a function of time t at $\beta = 5.85$, and $\kappa = 0.1585$ on the $8^3 \times 32$ lattice. As one sees, the plateau from which one can estimate the effective mass, is very narrow for point source, due to the reason mentioned above. When the smearing source is used, the width of the plateau changes with the smearing parameter r_0 . We tried many values of r_0 and found that when $r_0 \geq 16$, the effective mass is almost independent on r_0 where we observe the widest plateau. These figures imply that the smearing technique plays more important role for heavier hadrons to suppress the contamination of the excited states; Furthermore, one has to do careful study using the smearing technique, before doing simulation on a larger lattice.

We show the effective masses am_h of the light hadrons in Tab. 6 with smearing parameter $r_0 = 18$. The best fits to a range of points begin at $t_{min}=8$ to $t_{max}=16$. The masses are good agreement with the MILC previous results on the $16^3 \times 32$ lattice[21]. This means that finite size effects are small at this β and κ .

In Figs. 9 and 10, we compare our results (with $r_0 = 22$). for π mass squared, ρ mass, proton mass and Δ mass as a function of $1/\kappa$ for $\beta = 5.7$ with GF11 [22] on the same $8^3 \times 32$ lattice. The GF11 collaboration has 2439 configurations. Most results are consistent.

To determine the relation between the lattice spacing a and coupling β , one has to input the experimental value of a hadron mass (see Ref. [23] for details).

| Group | κ | Configs | Lattice | Source(s)→Sink | Fit Range | χ^2/dof | Mass |
|-------|----------|---------|------------------|-----------------------------|-----------|--------------|----------|
| MILC | 0.1450 | 23 | $20^3 \times 48$ | $a_1(P) \rightarrow a_1(P)$ | 6-11 | 1.7/4 | 1.312(8) |
| | | | | $1^{-+} \rightarrow 1^{-+}$ | 4-10 | 3.5/5 | 1.88(8) |
| | | | | $Q^4 \rightarrow 1^{-+}$ | 3-7 | 0.7/3 | 1.65(5) |
| ZSU | 0.1450 | 120 | $8^3 \times 32$ | $a_1(P) \rightarrow a_1(P)$ | 6-11 | 1.5/4 | 1.318(6) |
| | | | | $1^{-+} \rightarrow 1^{-+}$ | 4-10 | 4.2/6 | 1.87(10) |
| | | | | $Q^4 \rightarrow 1^{-+}$ | 3-7 | 1.2/3 | 1.65(2) |

Table 7: Effective masses for the ordinary P-wave a_1 meson and the exotic 1^{-+} meson for $\beta = 5.85$ between MILC and ZSU.

5.3 $a_1(P)$ and 1^{-+} hybrid meson masses

At $\beta = 5.85$ on the $8^3 \times 32$ lattice, 120 stored pure gauge configurations (see Tab. parameters) were re-used to study $a_1(P)$ and 1^{-+} hybrid meson masses. BiCGstab algorithm was employed to compute the quark propagators with Wilson fermions and the residue is of $O(10^{-7})$. Then we computed the correlation function using the sources and sinks in Tab. 4, from which the effective mass is extracted. Our results at $\kappa = 0.1450$ and $r_0 = 16$ are listed in Tab. 7, and compared with the MILC data[24].

6 Conclusions

We have demonstrated that a parallel cluster of PC type computers is an economical way to build a powerful computing resource for academic purposes. On an MPI QCD benchmark simulation it compares favorably with other MPI platforms.

We also present results for the light hadrons and 1^{-+} hybrid meson from lattice QCD. Such large scale simulations had usually required supercomputing resources, but now they were all done on our PC cluster. A more careful and systematic study of the smearing method is made. Our results for $\beta = 5.7$ and 5.85 are consistent well with the data obtained on supercomputers by other groups on the same or larger lattices. This implies that finite size effects are small at these β values.

To compare the lattice results with experiment, one needs to do simulations at larger β and carefully study the lattice spacing errors. According to the literature, there are strong finite size effects for the Wilson action at $\beta \geq 6.0$ and very larger lattice volume is required. In this aspect, it is more efficient to use the improved action and some progress has been reported in Refs. [25, 26].

In conclusion, we are confident that ZSU's Pentium cluster can provide a very flexible and extremely economical computing solution, which fits the demands and budget of a developing lattice field theory group. We are going to use the machine to produce more useful results of non-perturbative physics.

This work was in part based on the MILC collaboration's public lattice gauge theory code. (See reference [19].) We are grateful to C. DeTar, S. Gottlieb and D. Toussiant for helpful discussions.

References

- [1] Zhongshan University Computational Phys. and High Energy Phys. group,
<http://qomolangma.zsu.edu.cn>
- [2] X. Q. Luo, Comput. Phys. Commun. **94** (1996) 119.
- [3] X. Q. Luo and Q. Z. Chen, Mod. Phys. Lett. **A 11** (1996) 2435.
- [4] X. Q. Luo, Q. Z. Chen, S. H. Guo, X. Y. Fang and J. M. Liu, Nucl. Phys. **B(Proc. Suppl.)53**
(1997) 243.
- [5] X.Q. Luo, and E. B. Gregory, editors, "Non-Perturbative Methods and Lattice QCD", World
Scientific, Singapore (2001), 308 pages.
- [6] X. Q. Luo, Mod. Phys. Lett. **A16** (2001) 1615.
- [7] E. B. Gregory, S. H. Guo, H. Kroger and X. Q. Luo, Phys. Rev. **D62** (2000) 054508.
- [8] X. Q. Luo, E. B. Gregory, S. H. Guo and H. Kröger, arXiv:hep-ph/0011120.
- [9] C. Q. Huang, X. Q. Luo, H. Kroger and K. J. Moriarty, Phys. Lett. **A299** (2002) 483.
- [10] S. Catterall, and E. B. Gregory, Phys. Lett. **B487** (2000) 349.
- [11] H. Jirari, H. Kroger, X.Q. Luo, and K. Moriarty, Phys. Lett. **A281** (2001) 1.
- [12] L. A. Caron, H. Jirari, H. Kroger, X. Q. Luo, G. Melkonyan and K. J. Moriarty, Phys. Lett.
A288 (2001) 145.
- [13] H. Jirari, H. Kroger, X.Q. Luo, and K. Moriarty, S. Rubin, Phys. Rev. Lett. **86** (2001) 187.
- [14] <http://cesdis.gsfc.nasa.gov/linux/beowulf/beowulf.html>
- [15] William Gropp and Ewing Lusk, *Users Guide for mpich* (Argonne National
Laboratory:ANL/MCS-TM-ANL-96).
- [16] <http://www-unix.mcs.anl.gov/mpi/mpich>
- [17] Cray, Inc.
<http://www.cray.com/products/systems/crayt3e/1200data.html>
- [18] K. G. Wilson, Phys. Rev. **D10** (1974) 2445.
- [19] MILC Collaboration
<http://physics.indiana.edu/~sg/milc.html>
- [20] S. Gottlieb, Nucl. Phys. **B (Proc. Suppl.)94** (2001) 833.
- [21] K. M. Bitar *et al.*, Phys. Rev. D **46** (1992) 2169 [arXiv:hep-lat/9204008].

- [22] F. Butler, H. Chen, J. Sexton, A. Vaccarino and D. Weingarten, Nucl. Phys. **B430** (1994) 179.
- [23] Z. H. Mei, X. Q. Luo and E. B. Gregory, Chin. Phys. Lett. **19** (2002) 636.
- [24] C. W. Bernard *et al.* [MILC Collaboration], Phys. Rev. **D56** (1997) 7039.
- [25] Z. H. Mei and X. Q. Luo, arXiv:hep-lat/0206012.
- [26] X. Q. Luo and Z. H. Mei, Nucl. Phys. **B(Proc. Suppl.)119** (2003) 263. [arXiv:hep-lat/0209049].

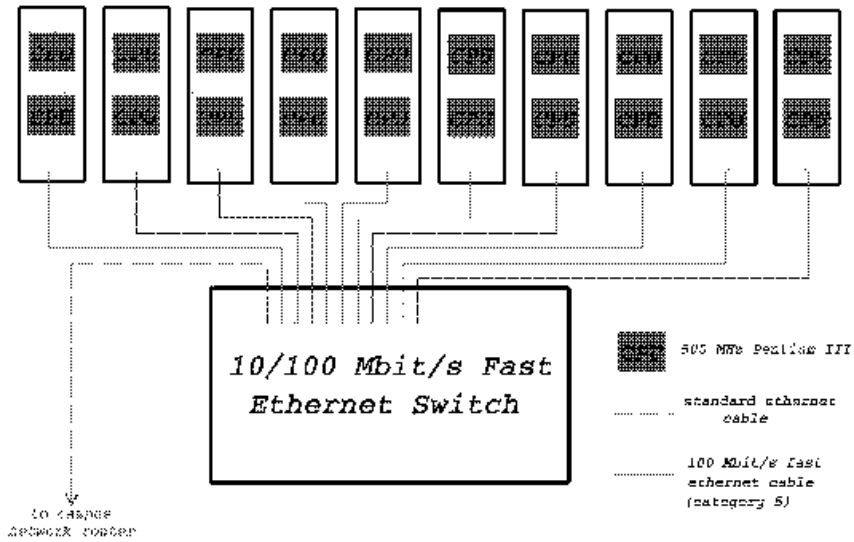


Figure 1: Schematic diagram of a parallel cluster.

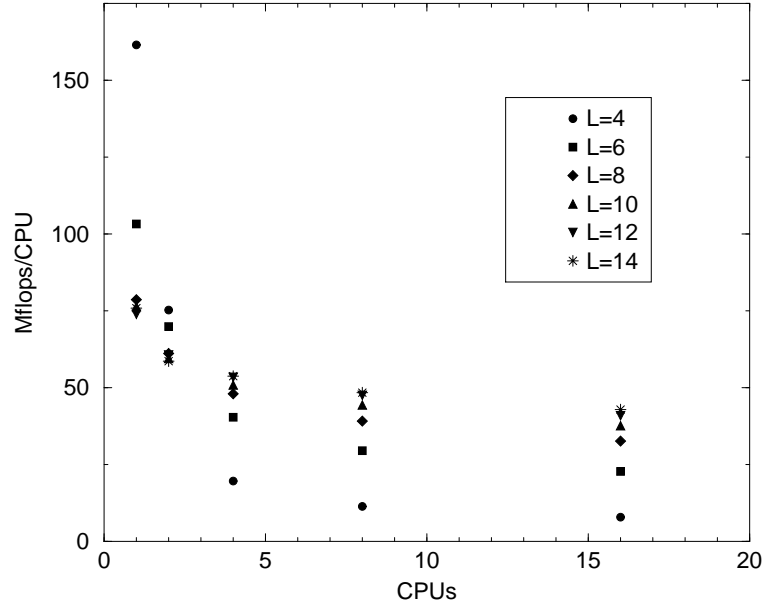


Figure 2: Performance (in Mega-Flops) per CPU versus the number of CPUs in the MILC QCD code benchmark.

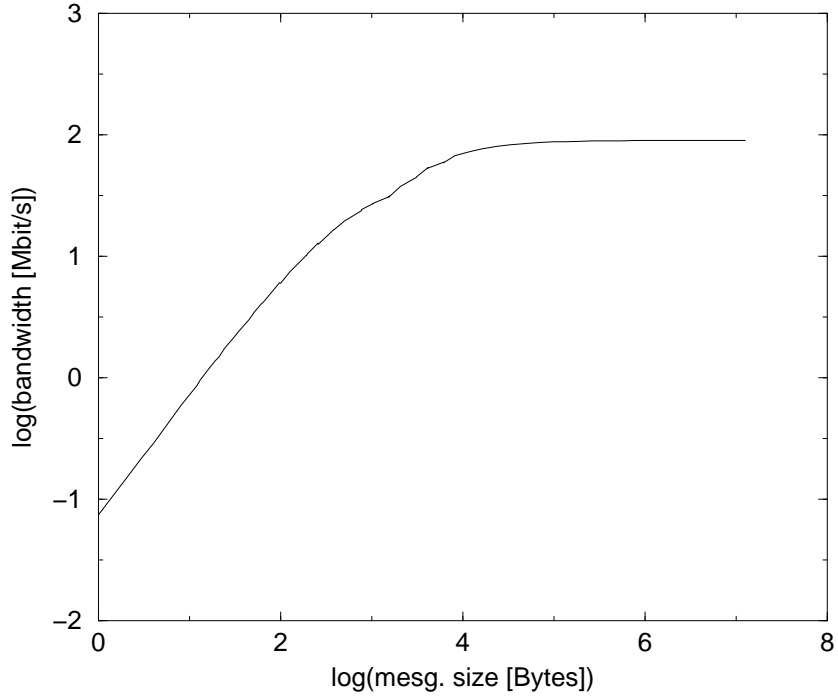


Figure 3: Communications bandwidth vs. message size.

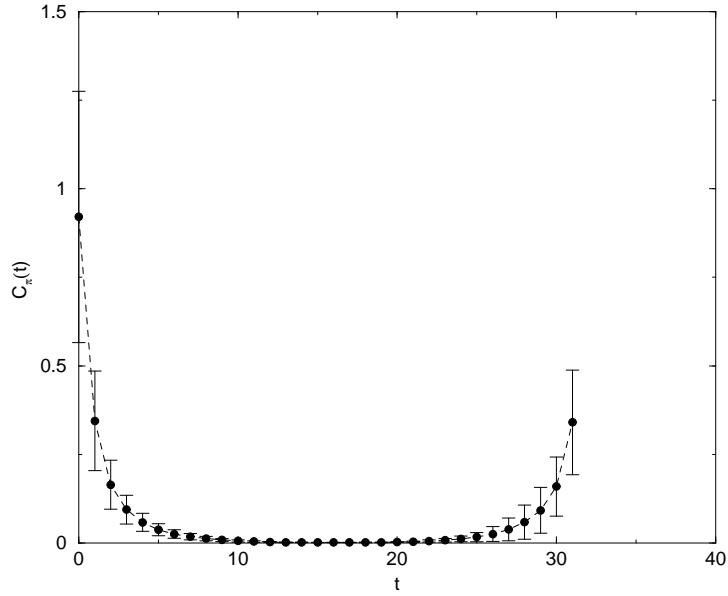


Figure 4: Green function of π at $\beta = 5.85$ and $\kappa = 0.1585$ on the $8^3 \times 32$ lattice. The error bars represent statistical errors determined by the Jackknife method.

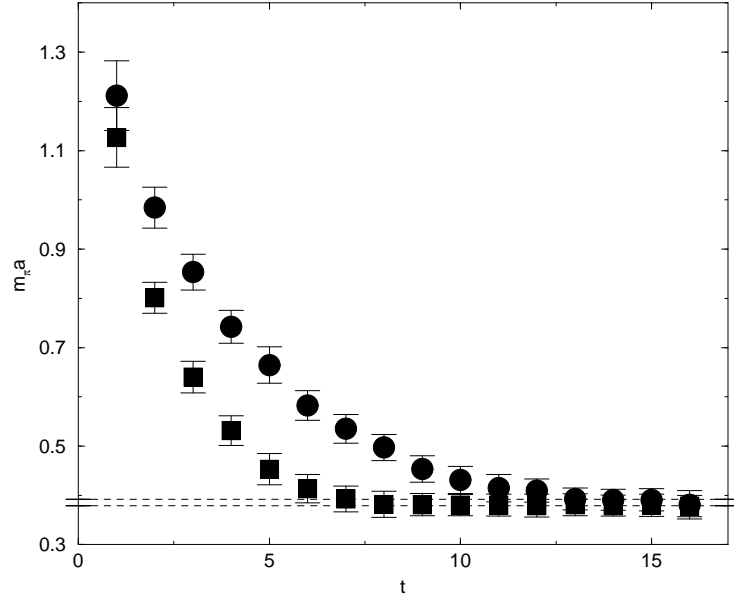


Figure 5: π effective mass fits to the correlation function at $\beta = 5.85$ and $\kappa = 0.1585$ and on the $8^3 \times 32$ lattice. Data for the point source, smearing source for $r_0 = 1$, and $r_0 = 18$ are labeled by circles and squares respectively (from top to bottom).

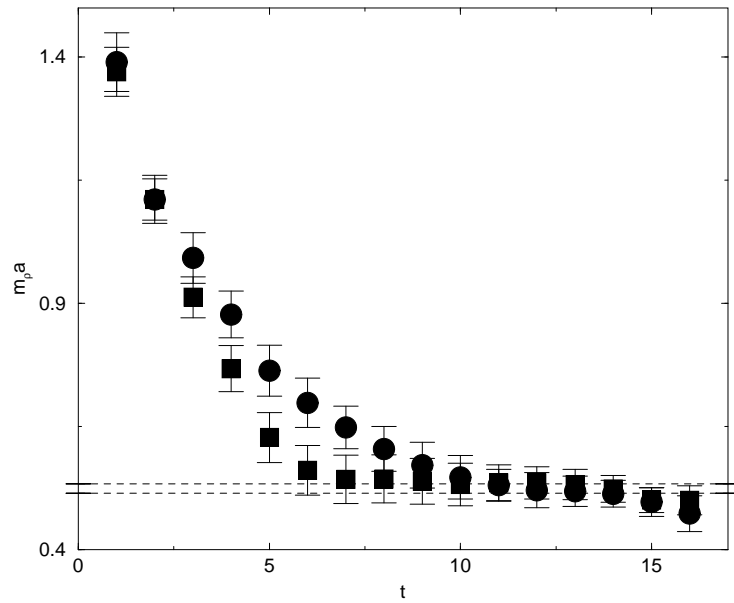


Figure 6: The same as Fig. 5, but for the ρ particle.

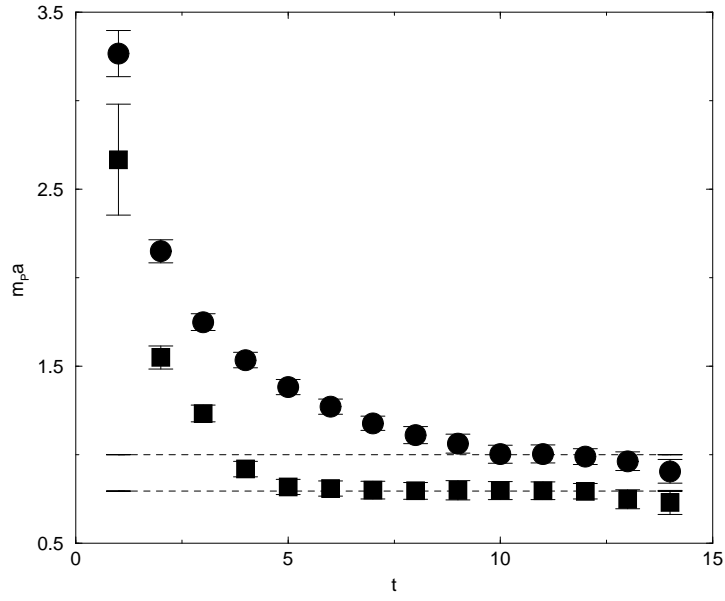


Figure 7: The same as Fig. 5, but for the proton particle.

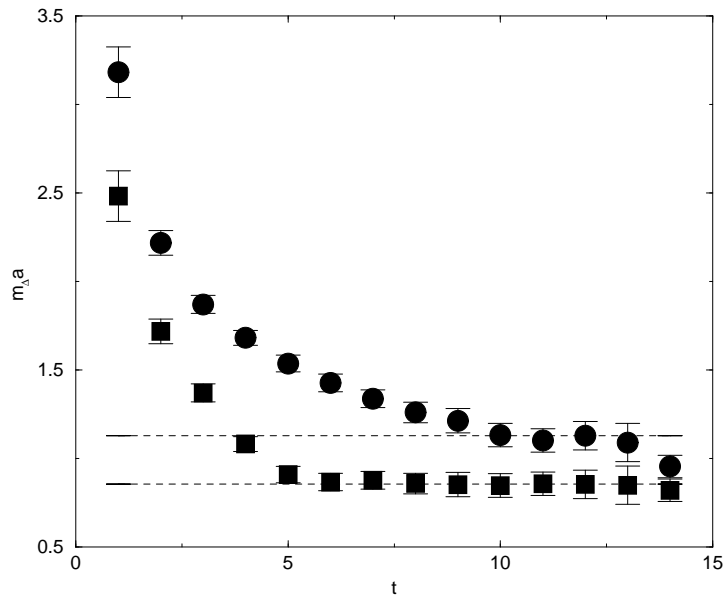


Figure 8: The same as Fig. 5, but for the Δ particle.

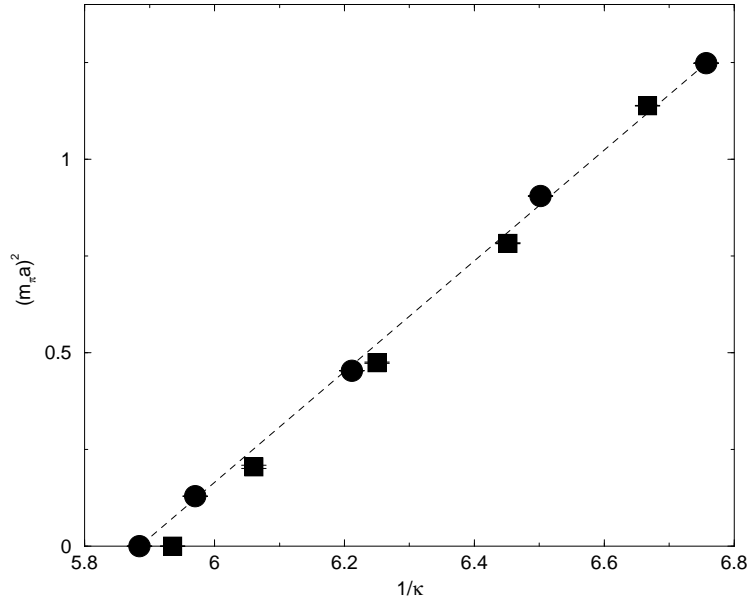


Figure 9: Pion mass squared as a function of $1/\kappa$ for $\beta=5.7$. ZSU's and GF11's results are labeled by circles and squares.

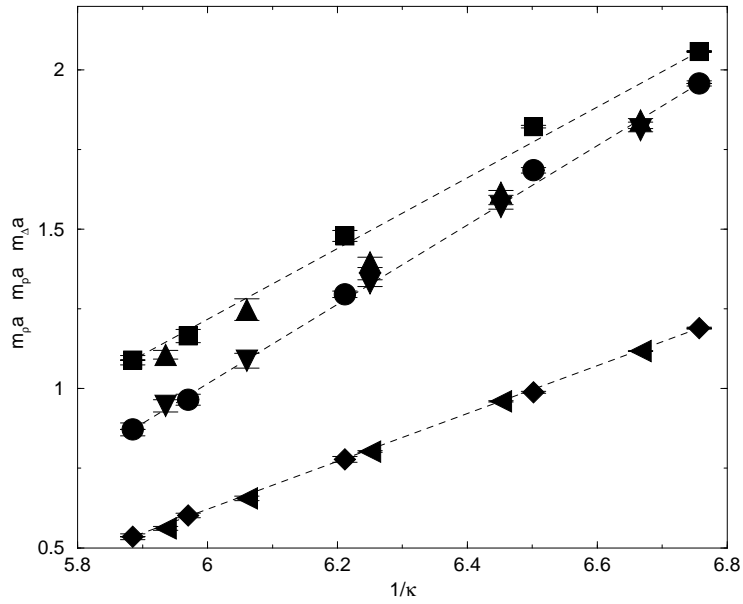


Figure 10: Effective mass of ρ (GF11: triangle left, ZSU: diamond), proton (GF11: triangle down, ZSU: circle), Δ (GF11: triangle up, ZSU: square) as a function of $1/\kappa$ for $\beta=5.7$. The points at the smallest value of $1/\kappa$ is the ZSU result extrapolated to the chiral limit.